Designing an electrochemical energy storage device using recycled Ti3C2Tx MXene and reduced graphene oxide spent wastewater adsorbents

Electrochimica Acta 540 (2025) 147176

Contents lists available at ScienceDirect

Electrochimica Acta

journal homepage: www.journals.elsevier.com/electrochimica-acta

Designing an electrochemical energy storage device using recycled $Ti_3C_2T_x$ MXene and reduced graphene oxide spent wastewater adsorbents

Marcelo A. Andrade [a,b], Olivier Crosnier [a,b], Patrik Johansson [c,d,e], Thierry Brousse [a,b,*]

[a] Nantes Université, CNRS, Institut des Matériaux de Nantes Jean Rouxel, IMN, 2 Rue de la Houssinière. Nantes, France
[b] Réseau sur le Stockage Electrochimique de l'Energie (RS2E), FR CNRS 3459, Hub de l'Energie, 15 Rue Baudelocque, 80039 Amiens, France
[c] Alistore-ERI European Research Institute, FR CNRS 3104, Hub de l'Energie, 15 Rue Baudelocque, 80039 Amiens, France
[d] Department of Physics, Chalmers University of Technology, SE-412 96 Gothenburg, Sweden
[e] Department of Chemistry – Ångström, Uppsala University, SE-751 20 Uppsala, Sweden

ARTICLE INFO

Keywords:
Reduced graphene oxide
MXene
Wastewater adsorbents
Heavy metals
Supercapacitor

ABSTRACT

This study presents an end-to-end approach for recycling hazardous waste heavy-metal-loaded adsorbents into electrode materials for electrochemical energy storage. Using reduced graphene oxide (rGO) and $Ti_3C_2T_x$ MXene as adsorbents for Hg^{2+}, Cu^{2+}, and Pb^{2+} from model wastewater solutions, we demonstrate their successful transformation into redox-active electrodes without any additional treatment. The recycled electrodes present superior capacity as compared to their pristine counterparts, while introducing distinct reversible redox features. Ultimately, the different recycled materials were assembled in full cell configurations, combining different metal-loaded adsorbents, yielding synergistic redox plateaus and an up to 50 % enhancement in the initial energy storage capacity, depending on the metal pair and electrolyte used. The versatility of this recycling strategy was demonstrated across three aqueous electrolytes, including a water-in-salt electrolyte, revealing tunable redox behavior dependent on both metal and electrolyte characteristics. Furthermore, using a more complex model wastewater solution, containing two different metal cations, leads to a multi-contaminant adsorbent that exhibits additive electrochemical responses, thereby establishing proof-of-concept for the reuse of real-world wastewater adsorbents into energy storage devices.

Introduction

Heavy metal contamination of water resources is a significant global environmental issue, as toxic metals such as mercury (Hg), lead (Pb), and copper (Cu) are well-known to bioaccumulate, posing severe risks to both ecosystems and human health [1]. Among various remediation technologies, adsorption is widely applied as a practical and efficient method for removing heavy metal ions from wastewater solutions due to its simplicity, cost-effectiveness, and high removal efficiency [2]. A range of adsorbent materials, from conventional activated carbons to advanced nanomaterials, have been explored for this purpose. In particular, nanoscale carbon-based materials such as reduced graphene oxide (rGO) and two-dimensional transition metal carbides (MXenes) show great performance in capturing heavy metals, due to their high specific surface area and tunable surface chemistries [3–5].

Once saturated with toxic metal cations, the spent adsorbents themselves become hazardous waste requiring careful handling. Unlike organic pollutants, heavy metals cannot be degraded and remain immobilized on the sorbent, raising concerns of secondary pollution if these materials are simply discarded. This challenge has motivated research into strategies for regenerating or repurposing spent adsorbents to "close the loop" on the remediation process [6–9].

One attractive approach is to recycle heavy metal-loaded adsorbents by converting them into functional electrode materials for electrochemical energy storage. We recently demonstrated that an rGO-based adsorbent saturated with mercury from wastewater can be directly repurposed as a highly performant electrode for electrochemical capacitors [10]. In that study, a three-dimensional rGO foam was used to adsorb >95 % of Hg^{2+} ions from a model polluted water, achieving an average loading of *ca.* 240 mg of Hg per g of rGO, among the highest adsorption capacities reported. The resulting mercury-loaded rGO (denoted rGO/Hg_{ads}) exhibited distinct redox activity associated with Hg species and delivered a ~15 % higher charge-storage capacity as compared to pristine rGO. Likewise, other high-surface conductive

* Corresponding author.
E-mail address: thierry.brousse@univ-nantes.fr (T. Brousse).

https://doi.org/10.1016/j.electacta.2025.147176
Received 16 July 2025; Received in revised form 15 August 2025; Accepted 15 August 2025
Available online 16 August 2025

adsorbents, such as MXenes, could be recycled similarly once loaded with heavy metals.

The most widely studied MXene, $Ti_3C_2T_x$, has been used in both wastewater treatment and energy storage domains, due to its high adsorption efficiency and electrochemical redox activity. Their abundant, synthesis-dependent, polar surface terminations result in a hydrophilic, negatively charged surface with numerous active sites for binding heavy metal cations via electrostatic interaction, surface complexation, or ion-exchange mechanisms [11]. Likewise, these surface groups serve as redox-active sites in energy storage. Pseudocapacitive charge storage has been reported from oxygen-terminated MXene electrodes, which readily bond with electrolyte ions, in contrast to less-active fluorine-terminated surfaces. For instance, $Ti_3C_2T_2$ MXene electrodes inherently provide around 200 $F{\cdot}g^{-1}$ via pseudocapacitive ion intercalation, while post-synthesis replacement of -F with -O was shown to boost its capacitance *ca.* 2.5-fold by enhancing wettability and creating additional proton-binding sites [12,13]. Notably, hybrid devices that combine Faradaic and double-layer charge storage can exceed these values by benefiting from the redox activity of both the MXene structure and the embedded metal species [14].

To put into perspective, traditional activated carbon (AC) electrodes typically deliver on the order of 150 $F{\cdot}g^{-1}$ in aqueous electrolytes [15]. Graphene-derived carbons, such as rGO, can achieve significantly higher values, often a few hundred $F{\cdot}g^{-1}$ when optimized [16]. Hydrothermally prepared rGO hydrogels, used as binder-free symmetric supercapacitor electrodes, delivered 268 $F{\cdot}g^{-1}$ at 0.3 $A{\cdot}g^{-1}$ and retained 222 $F{\cdot}g^{-1}$ at 10 $A{\cdot}g^{-1}$ in 6 M KOH [17]. The choice of electrolyte is also essential for exploring and eventually optimizing the electrochemistry. A conventional acidic electrolyte, such as 1 M H_2SO_4, offers high ionic conductivity and proton-mediated redox enhancement, but limits the useful potentials from 0 V to 1.23 V *vs.* SHE, due to water electrolysis and hence a narrow electrochemical stability window (ESW). In contrast, the use of a "water-in-salt electrolyte" (WiSE) can dramatically expand the ESW well above 2 V, enabling higher energy density [18]. Moreover, the pH and the electrolyte composition can be tailored to match the chemistry of the adsorbed cation(s).

In this work, adsorbents containing different heavy metal cations were systematically explored as recycled electrodes and combined with different electrolytes, aiming to optimize capacity, potential range, and cycling stability of an electrochemical full cell. A step closer to meeting practical application requirements was taken with the design of this tunable full cell, all while ensuring the approach remains viable for real-world wastewater solutions/streams and cation contaminations.

Results and discussion

Electrochemical energy storage

rGO and the MXene $Ti_3C_2T_x$ were initially tested as adsorbents for wastewater contaminants. Given the current literature for heavy metal removal, as well as the expected redox potentials for each of the heavy metals, the MXene was selected for Cu^{2+} cation adsorption, and rGO for all three Hg^{2+}, Pb^{2+}, and Cu^{2+} cations [19]. Solutions containing 300 $mg{\cdot}L^{-1}$ of either Hg^{2+}, Cu^{2+}, or Pb^{2+} cations were used as artificial wastewater to evaluate the adsorption performance using a constant dose of 100 $mg{\cdot}L^{-1}$ at pH 5.5, and the results (Table S1) are in agreement with the literature [3,5,10]. The high adsorption capacity of rGO, particularly towards mercury cations – reaching almost 40 wt. % – demonstrates its potential use as an efficient adsorbent as well as the importance of recycling this hazardous material at its end-of-life.

The metal-loaded adsorbents were recovered after being saturated, then filtered and lyophilized to preserve their microporosity for reuse [10]. The elemental composition was investigated using energy-dispersive X-ray spectroscopy (EDX) analysis (Table S2) coupled with a scanning electron microscope (SEM). The SEM micrographs of pristine rGO and $Ti_3C_2T_x$ reveal very porous microstructures, with the former being mostly amorphous and the latter being layered (Fig. S1). No changes were observed in the overall microstructure of any of the materials after adsorption, demonstrating that the recovery method was effective in maintaining porosity.

The 40 wt. % oxygen content measured by EDX for $Ti_3C_2T_x$ was indicative of its high oxygen-containing functional surface groups, typical of the MILD synthesis method [20]. Usually, the more oxygenated the surface of the MXene, the stronger its affinity for metal ions. Hydroxyl and carboxyl groups are known for trapping heavy metal cations in "potential wells" by coordination to their deprotonated form. In contrast, more inert fluorine terminations tend to lower the adsorption capacity [11]. In the case of rGO, its partially reduced structure leads to oxygenated functional groups, which reach 36 wt. % for the pristine adsorbent [10]. The presence of these groups has been demonstrated to translate into two uptake mechanisms for rGO [21,22]. First, a rapid inner-sphere chemisorption at deprotonated hydroxyl and carboxyl sites occurs. As these higher-energy sites fill, weaker electrostatic interactions with raphemic domains increasingly contribute to the overall capture. Consistently, batch data follow a Freundlich isotherm ($1/n \approx 0.2$) and fast Elovich kinetics, evidencing a heterogeneous energy landscape that enables high capacities in the order of hundreds of $mg{\cdot}g^{-1}$ for this material [23].

Self-standing electrodes were made using the recycled adsorbents, and subsequently, these were electrochemically studied using Swagelok cells.

The cyclic voltammetry using a 1 M H_2SO_4 electrolyte shows capacitive behavior for the pristine rGO, combined with some pseudocapacitance for pristine $Ti_3C_2T_x$ derived from termination groups' redox reactions, resulting in a mostly rectangular shapes with no prominent peaks (Fig. 1a) [24]. Upon adsorption of specific heavy metals by the electrodes, the rGO/Hg_{ads} shows reversible redox peaks at 0.62 V *vs.* SHE, rGO/Cu_{ads} presents a pair of peaks at 0.18 V *vs.* SHE (Fig. 1b and c, respectively), while $Ti_3C_2T_x/Cu_{ads}$ shows a similar pair of redox peaks at 0.20 V *vs.* SHE (Fig. 1d). Upon cycling, the redox peaks decrease in intensity, leading to capacity fading and ultimately a mainly non-faradaic response. rGO/Pb_{ads} and $Ti_3C_2T_x/Pb_{ads}$ were also tested in the same electrolyte, however, no redox activity was evidenced within this ESW (Fig. S2). That is due to the Pb^{2+}/Pb(s) redox couple occurring in more negative potentials than the expected stability for water at pH 0, meaning that accessing this couple would coincide with H_2 evolution [25].

The electrochemical behavior corresponds to the Pourbaix diagram potentials of the redox reactions of the adsorbed cationic species at pH 0:

$$Hg^{2+} + e^- \rightleftharpoons Hg^+ \; E_{red}^\circ = 0.61 \text{ V } \textit{vs.} \text{ SHE}^{25} \qquad \text{(Reaction 1)}$$

$$Cu^{2+} + e^- \rightleftharpoons Cu^+ \; E_{red}^\circ = 0.17 \text{ V } \textit{vs.} \text{ SHE}^{25} \qquad \text{(Reaction 2)}$$

The expected potential for both reactions is from the divalent cation to the monovalent cation, with no metallic forms present. Hence, dissolution of cations upon cycling could explain the capacity fading, leading us to explore how to improve the cyclability by tuning the electrolyte ionicity (see below).

The added faradaic redox activity not only enriches the electrochemistry but also contributes to the total electrode capacity, especially as the electrochemical double layer capacitance (EDLC) is maintained. Pristine rGO presents a maximum anodic cycling capacity of 185 $C{\cdot}g^{-1}$, while $Ti_3C_2T_x$ has a capacity of 110 $C{\cdot}g^{-1}$ due to its narrower ESW (Fig. S3). The presence of Hg^{2+} in rGO/Hg_{ads} increases the initial capacity up to 215 $C{\cdot}g^{-1}$, while Cu^{2+} cations in rGO/Cu_{ads} raise the capacity up to 202 $C{\cdot}g^{-1}$. The same trend is observed for $Ti_3C_2T_x/Cu_{ads}$, with a capacity of 120 $C{\cdot}g^{-1}$.

Considering that the electrode mass is normalized by the mass of total active material, the adsorbed metals account as dead weight for the EDLC capacity contribution. Hence, upon metal loss, the capacities, mostly non-faradaic, are smaller than expected for the pristine and pure adsorbents. Taking that into account, and the measured adsorbed mass

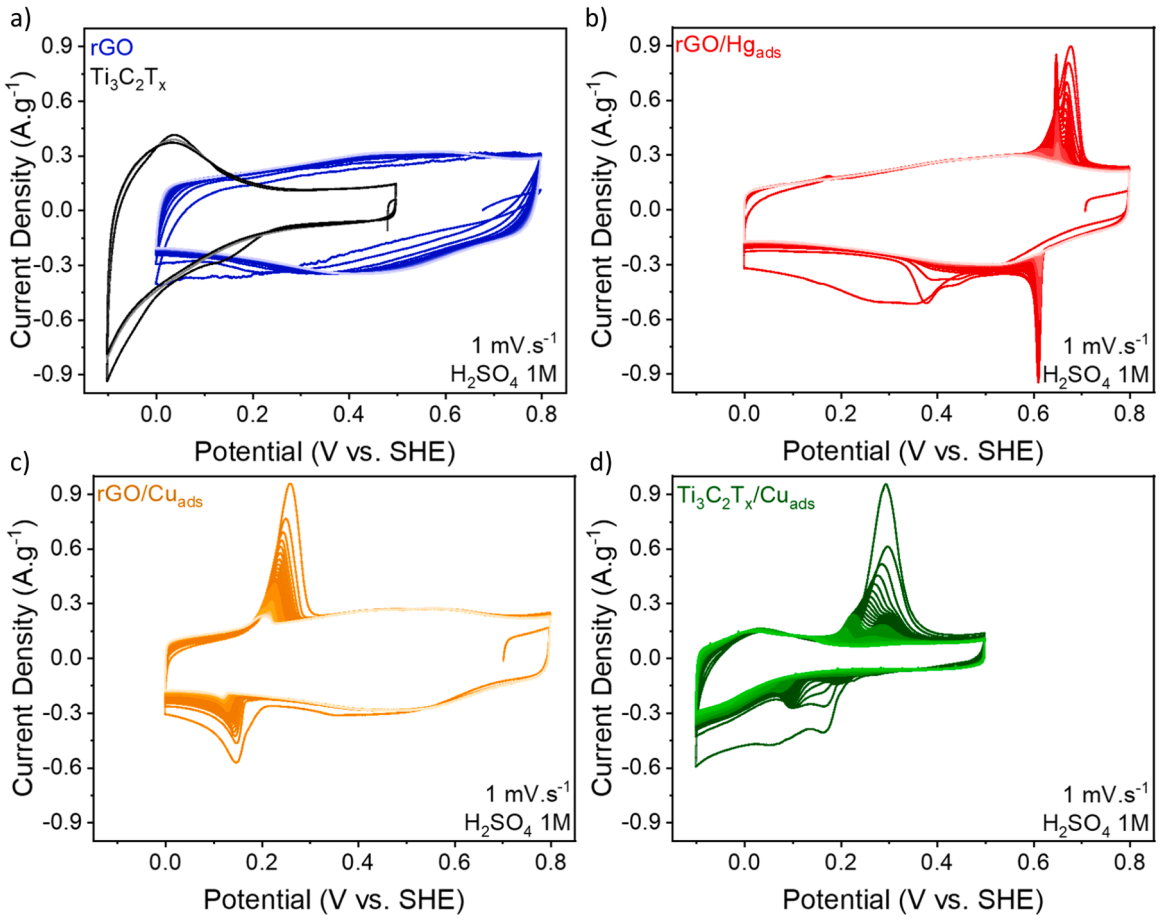

Fig. 1. Cyclic voltammetry at 1 mV·s^{-1} in 1 M H_2SO_4 of: a) pristine rGO (blue) and $Ti_3C_2T_x$ (black), b) rGO/Hg_{ads}, c) rGO/Cu_{ads}, and d) $Ti_3C_2T_x/Cu_{ads}$.

of each cation (Table S2), the faradaic capacity of rGO/Hg_{ads} corresponds to a one-electron exchange of 54 % of its adsorbed Hg^{2+} cations, while for $Ti_3C_2T_x/Cu_{ads}$ it is of 23 % of its adsorbed Cu^{2+}cations, the same as for rGO/Cu_{ads} (Table S3). This means that a considerable portion of the adsorbed cations is not contributing to the redox activity.

The interest in being able to adsorb different cations by various adsorbents goes beyond the electrode capacity increase. By selectively screening specific adsorbents coming from cleaning different sources of wastewater, full cells can be assembled by using the diversity of redox potentials provided. Following this logic, a device was assembled using rGO/Hg_{ads} as the positive (working) electrode (WE) and $Ti_3C_2T_x/Cu_{ads}$ as the negative (counter) electrode (CE), together with a reference electrode (RE) of $Hg/HgSO_4$ in saturated K_2SO_4, enabling us to monitor the potentials of these electrodes, and benchmarked using analogous cells using pristine adsorbents (Fig. 2).

The potentials of both electrodes made of pristine adsorbents present a mostly linear variation with the current density (applied with respect to the active mass of the lighter electrode) (Fig. 2a). The respective full cell voltage also shows a linear variation with the current density up to 1 V (Fig. 2b). For the electrodes containing adsorbed cations, there are more features. A plateau is present at 0.6 V *vs.* SHE for the rGO/Hg_{ads} electrode and at 0.2 V *vs.* SHE for the $Ti_3C_2T_x/Cu_{ads}$ electrode, confirming the presence of both metal cations' redox reactions in the same cell. The full cell voltage was also incremented with a plateau corresponding to the occurrence of the redox reactions, increasing the capacity of the full cell up to 20 % as compared to the device using pristine absorbents as electrodes.

The smaller total capacity of the MXene-derived electrode as compared to the rGO electrode derives from the need to use a much higher electrode mass on the negative electrode to balance the cell capacity. This could hinder the exploration of different metal redox reactions, due to the limited potential window, even though MXenes can be great adsorbents and redox materials precursors themselves [26–29]. To overcome this issue, the same type of adsorbent was used in both positive and negative electrodes, while adsorbing different metals. rGO is able to adsorb almost twice as much Cu^{2+}cations as $Ti_3C_2T_x$, reaching >8 wt. %, and was tested as anode in a full cell *vs.* a rGO/Hg_{ads} cathode (Fig. 2c and d).

Here, the potential plateau for the rGO/Hg_{ads} redox reaction is clearly observed, as well as for copper. The use of the same base material, with the same capacitance, in both positive and negative electrodes allows for a more symmetric distribution of the capacity, as evidenced by the dashed blue lines. On the other hand, the higher capacity provided by the rGO/Hg_{ads} ended up limiting the potential window for rGO/Cu_{ads}, even though the capacities overall are higher than for $Ti_3C_2T_x/Cu_{ads}$ (Table S3). The influence of the adsorbed cations is evident by the presence of a plateau in the cell voltage as well, which initially increased the cell capacity from 108 to 168 C·g^{-1} – about 50 % – at 100 mA·g^{-1} (Fig. 2d).

To further explore other adsorbed metal cations in rGO, such as Pb^{2+} cations, different electrolytes were investigated to increase the ESW. More specifically, we employed 20 m potassium acetate (Kac), a water-in-salt electrolyte (WiSE) providing an ESW of 1.6 V for rGO (Fig. 3).

The cyclic voltammetry using the 20 m Kac WiSE favors the exploration of redox reactions beyond the usual water stability range. Pristine rGO, as expected, presents a mostly rectangular shape voltammogram, typical of EDLC behavior, reaching an anodic capacity of 360 C·g^{-1} due to the enlarged potential window (Fig. 3a). The mercury oxidation reaction for the rGO/Hg_{ads} electrode is a very sharp peak at 0.3 V *vs.* SHE, while its reduction is more likely spread over a range of potentials from

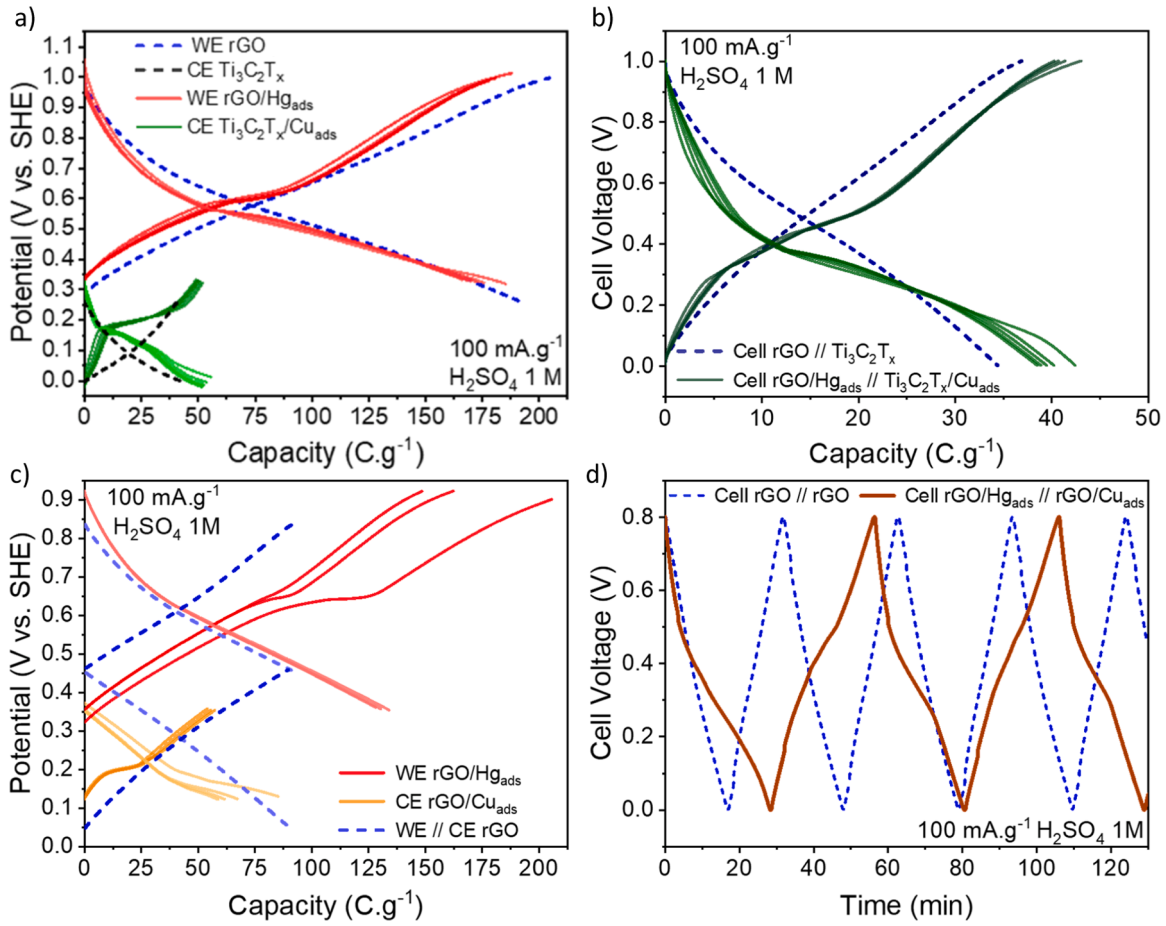

Fig. 2. Galvanostatic charge and discharge (GCPL) of a full device using a 3-electrode set-up in 1 M H_2SO_4 with a current density of 100 mA·g^{-1}, using a reference electrode of Hg/$HgSO_4$ in saturated K_2SO_4. The dashed lines show cells using pristine adsorbent electrodes as both anode and cathode. The solid lines show the cells cycled under the same conditions, using metal-loaded adsorbents. A) rGO/Hg_{ads} as the positive working electrode (WE), and $Ti_3C_2T_x$/Cu_{ads} as the negative counter electrode (CE), with the cell voltage shown in b). c) WE (positive) is rGO/Hg_{ads} and CE (negative) is rGO/Cu_{ads}, with the cell voltage shown in d).

0.2 to −0.1 V *vs.* SHE (Fig. 3b). For the rGO/Cu_{ads} electrode, the copper redox reactions are still present, now shifted towards lower potentials, −0.1 V *vs.* SHE, due to the more alkaline character of the electrolyte, but still with well-defined peaks (Fig. 3c). The wider voltage range also allowed detection of the redox reaction of lead in rGO/Pb_{ads}, with the appearance of a modest redox pair at −0.55 V *vs.* SHE (Fig. 3d). The supposed electrochemical reactions at pH 9 are as follows:

$Hg(OH)_2 + 2e^- \rightleftharpoons Hg^0_{(aq)}$ $E_{red}^\circ = 0.61$ V *vs.* SHE [25] (Reaction 3)

$Cu(OH)_2 + e^- \rightleftharpoons Cu^+$ $E_{red}^\circ = 0.05$ V *vs.* SHE [25] (Reaction 4)

$Cu^+ + e^- \rightleftharpoons Cu^0$ $E_{red}^\circ = -0.09$ V *vs.* SHE [25] (Reaction 5)

$PbOH^+ + 2e^- \rightleftharpoons Pb^0$ $E_{red}^\circ = -0.55$ V *vs.* SHE [25] (Reaction 6)

The shoulder on the oxidation peak of lead could relate to a two-step electron transfer reaction up to its divalent form. To take advantage of the difference in potential between lead and mercury redox reactions, a full cell configuration was explored using rGO/Hg_{ads} as the positive electrode and rGO/Pb_{ads} as the negative electrode, and a constant cycling current of 100 mA·g^{-1} (Fig. 4), again benchmarked using the same set-up and conditions but with pristine rGO electrodes.

The positive WE shows a slightly higher capacitance and hence capacity as compared to when using the acidic electrolyte, but in addition, the overall mass distribution is quite symmetric. The cell discharge capacity in the case of pristine adsorbents was 55 C·g^{-1}, normalized by the mass of both electrodes. For the metal-loaded adsorbents, clear potential plateaus can be seen for each electrode (Fig. 4a), corresponding to the redox reactions seen in the cyclic voltammograms and initially increasing the discharge capacity from 52 to 68 C·g^{-1}, with a voltage plateau at 0.75 V.

The key to exploring the most performant out of the recycled adsorbents is electrolyte choice and electrode engineering. The direct repurposing of the recovered powder into electrodes is basically a zero-energy input process, drastically increasing the importance of the right choice of electrolyte – and finally, we present an attempt to enhance the cyclability using a 2 M sodium carbonate (Na_2CO_3) electrolyte (Fig. 5).

A wide voltage window of 1.5 V was chosen to encompass the redox potentials of all the cations, but admittedly, the hydrogen and oxygen gas evolution reactions were already present within the lower and upper potential limits (Fig. 5a). The mercury redox reaction is present at 0.3 V *vs.* SHE as very broad peaks with low intensity, related to Reaction 3, but shifted as we are now at pH 11. Similarly, rGO/Cu_{ads} presents the redox pair related to Reaction 5, still with very broad and intense peaks. Finally, rGO/Pb_{ads} shows very intense and sharp redox peaks at – 0.6 V *vs.* SHE:

$Pb(OH)_3^- + 2e^- \rightleftharpoons Pb^0$ $E_{red}^\circ = -0.60$ V *vs.* SHE [25] (Reaction 7)

The presence of these sharp peaks also increased the cycling stability of rGO/Pb_{ads}, lasting up to 50 % until cycle 15. Once again, a split of the oxidation peak into two peaks at −0.51 V *vs.* and −0.48 V *vs.* SHE was observed, and hence the charge transfer must occur in two separate steps for the re-oxidation, while the reduction is a single broad peak. It is clear that the electrolyte composition plays a crucial role not only in the redox behavior of the adsorbed metals, but in the stability of these recycled

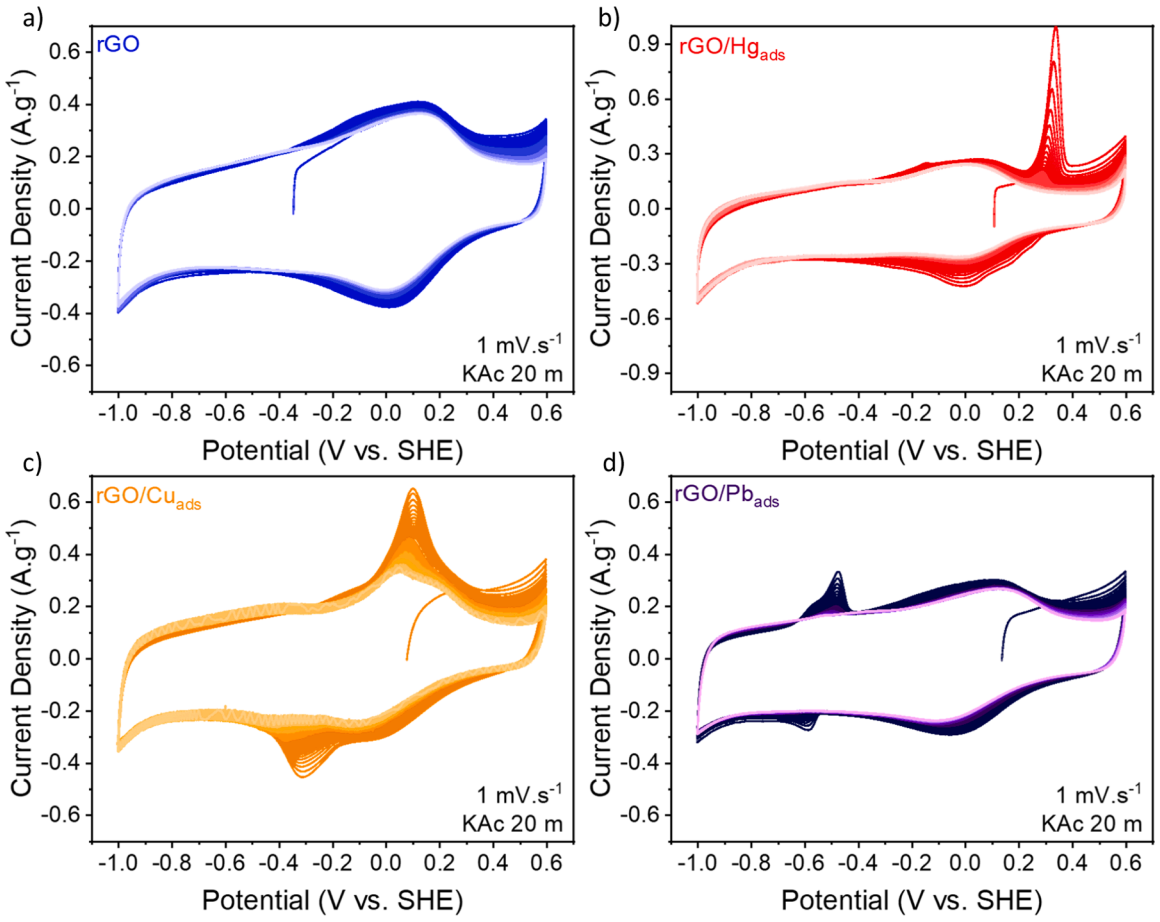

Fig. 3. Cyclic voltammetry at 1 mV·s^{-1} using the WiSE 20 m Kac of: a) pristine rGO, b) rGO/Hg_{ads}, c) rGO/Cu_{ads}, and d) rGO/Pb_{ads}.

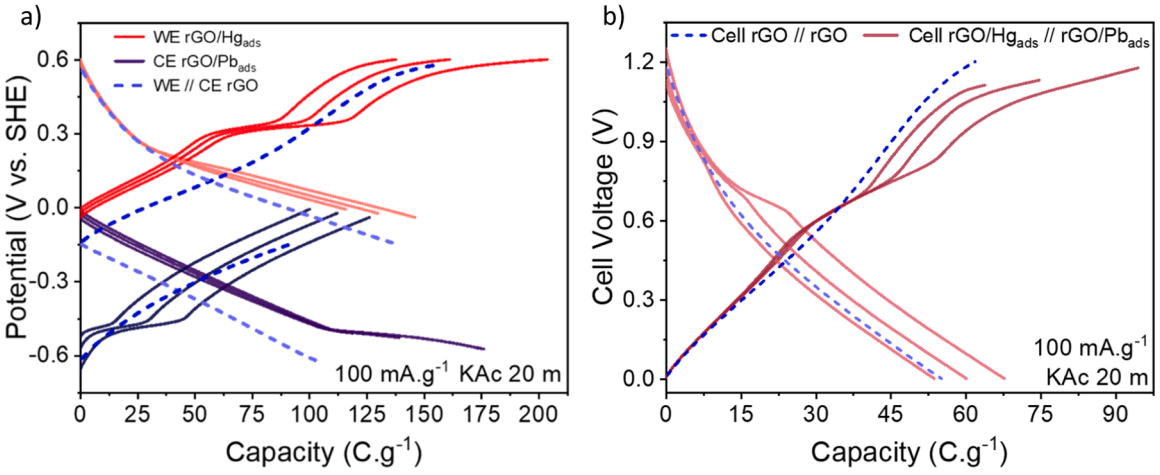

Fig. 4. Galvanostatic charge and discharge (GCPL) of a full cell device using a 3-electrode set-up using the WiSE 20 m Kac and a current density of 100 mA·g^{-1}. The dashed lines show a cell using pristine rGO as both anode and cathode. The solid lines show one cell cycled under the same conditions, using rGO/Hg_{ads} as the positive WE, while the negative CE was rGO/Pb_{ads}, and the RE was Hg/$HgSO_4$ in saturated K_2SO_4.

electrodes. Some of the metals tend to dissolve faster in acidic electrolytes, while also presenting more prominent redox peaks. More concentrated electrolytes, on the other hand, can increase the lifespan of the faradaic contribution of the electrodes to tens of cycles. A significant advantage of these materials, however, is that they are originally designed for good supercapacitor behavior, and still exhibit a significant double-layer capacitance after prolonged cycling (Fig. S4).

Lastly, the rGO adsorbent was used in a more complex simulated wastewater solution containing 300 mg·L^{-1} of two metal cations: Hg^{2+} and Cu^{2+}. The higher affinity of rGO towards mercury was confirmed by its adsorption capacity being almost 15 times higher than that of copper: $q_{eq/Hg}$ = 388 mg·g^{-1} vs. $q_{eq/Cu}$ = 26 mg·g^{-1} (Table S1). By cycling in different electrolytes, the electroactivity of the adsorbed cations in rGO/$HgCu_{ads}$ was evaluated (Fig. 6).

The electrochemical response equals the sum of the EDLC contribution coming from the rGO with the redox reactions of Hg^{2+} and Cu^{2+}

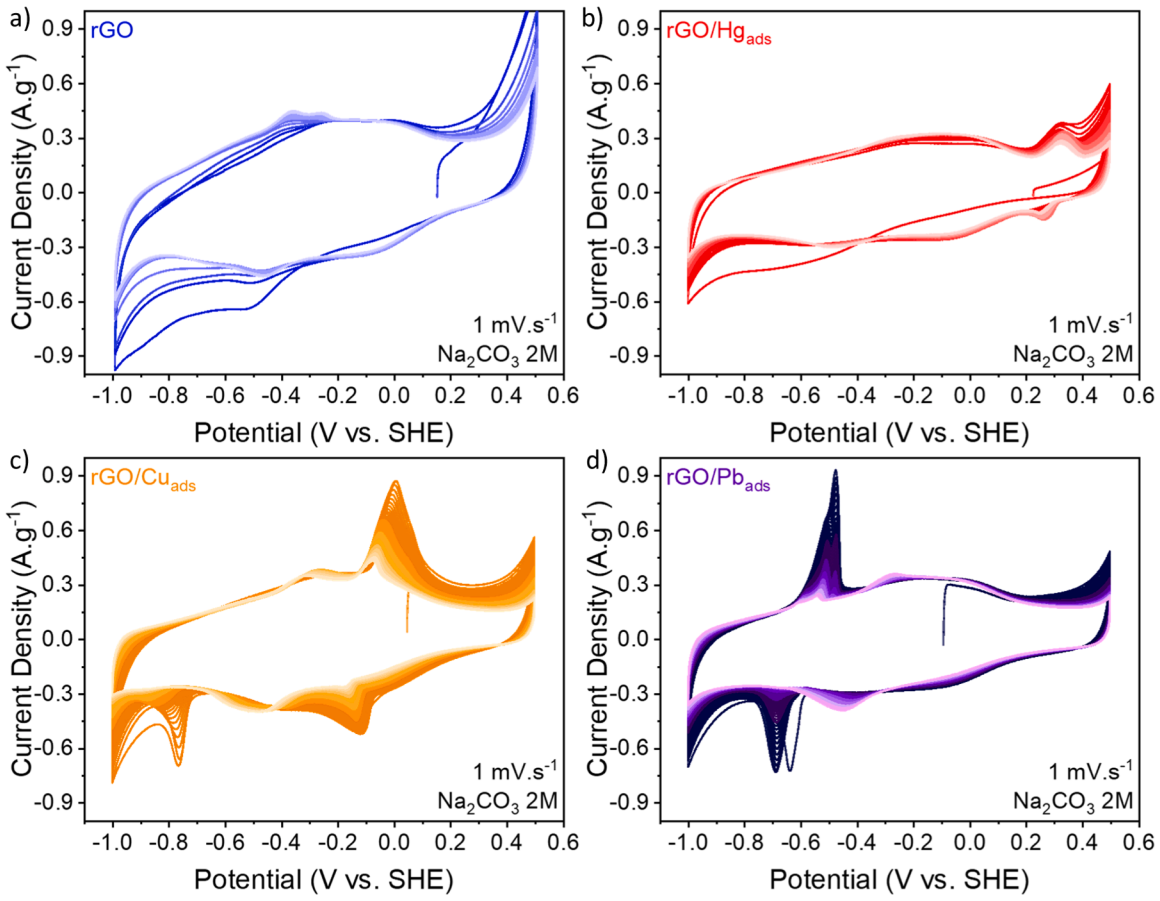

Fig. 5. Cyclic voltammetry at 1 mV·s^{-1} in 2 M Na_2CO_3 of: a) pristine rGO, b) rGO/Hg_{ads}, c) rGO/Cu_{ads}, and d) rGO/Pb_{ads}.

cations, which maintain the same peak positions. Hence, more complex wastewater solutions can be applied to synergistically contribute to the final electrochemical response, paving the way towards realistic direct recycling of wastewater adsorbents.

Experimental

Adsorption experiments

Isothermal adsorption

A stock solution of 1000 mg·L^{-1} of Hg^{2+} cations was prepared by dissolving the appropriate mass of mercury nitrate ($Hg(NO_3)_2{\cdot}H_2O$, purity > 98 %, Thermo Scientific) in 500 mL of deionized (DI) water. The same method was applied to prepare standard solutions of other metal cations, using nitrate salts of lead ($Pb(NO_3)_2$, 99 %, Alfa Aesar) or copper ($Cu(NO_3)_2{\cdot}3H_2O$, 99 %, Acros Organics™). Solutions of 300 mg·L^{-1} were obtained by appropriate dilution with DI water. The complex solution containing 300 mg·L^{-1} of both Hg^{2+} and Cu^{2+} cations was prepared by the appropriate mixing and dilution of the stock solutions of these metals. The pH was adjusted to 5.5 using 0.1 M NaOH or 0.1 M HNO_3 when needed.

Isothermal adsorption

Adsorption tests were conducted by placing approximately 10 mg of dry adsorbent into 25 mL glass vials. The powder was put under vacuum using a Schlenk-like setup to ensure full impregnation with the adsorbate solution. Then, 20 mL of a 300 mg·L^{-1} heavy metal solution was introduced into the vial. Stir bars were added, and the mixture was kept under constant stirring in a temperature-controlled water bath overnight.

Concentration analysis

After the adsorption process, the stir bar was removed, and the adsorbent/wastewater suspension was vacuum-filtered through PVdF membranes (0.45 μm, hydrophilic, Durapore) to recover the metal-loaded adsorbent and to determine the remaining metal concentration in solution. The filtered powder was collected and dried for electrode fabrication, while the filtrate was transferred to clean vials for elemental analysis via X-ray fluorescence (XRF). The metal content in the aqueous phase was quantified using a calibrated energy-dispersive XRF spectrometer (EDXRF Epsilon 1, Malvern PANalytical). The residual concentration and adsorption capacity were calculated relative to a blank control, where the same procedure – vacuum treatment, temperature bath, and filtration – was conducted in the absence of adsorbent.

Synthesis procedures

Synthesis of Graphene Oxide (GO) and reduced Graphene Oxide (rGO). Both GO and rGO were prepared according to a previously reported method [10]. In brief, GO was synthesized from graphite powder using the improved Hummers method and stored as an aqueous suspension at a concentration of 1 mg mL^{-1}. A 35 mL aliquot of this suspension was transferred into 50 mL Teflon-lined autoclaves and subjected to hydrothermal treatment at 180 °C for 12 h. The resulting rGO foam was thoroughly rinsed with deionized water and subsequently lyophilized.

Synthesis of MXenes [20,30]. Titanium aluminum carbide 312 (Ti_3AlC_2 MAX phase, Sigma Aldrich, purity ≥ 90 %, particle size ≤ 40 μm) was treated overnight (~18 h) at room temperature using 9 M hydrochloric acid (HCl, ~37 %, Fisher Chemical), with an acid-to-MAX ratio of 25 mL per 1 g. This process aimed to eliminate intermetallic impurities and non-stoichiometric phases from the initial material.

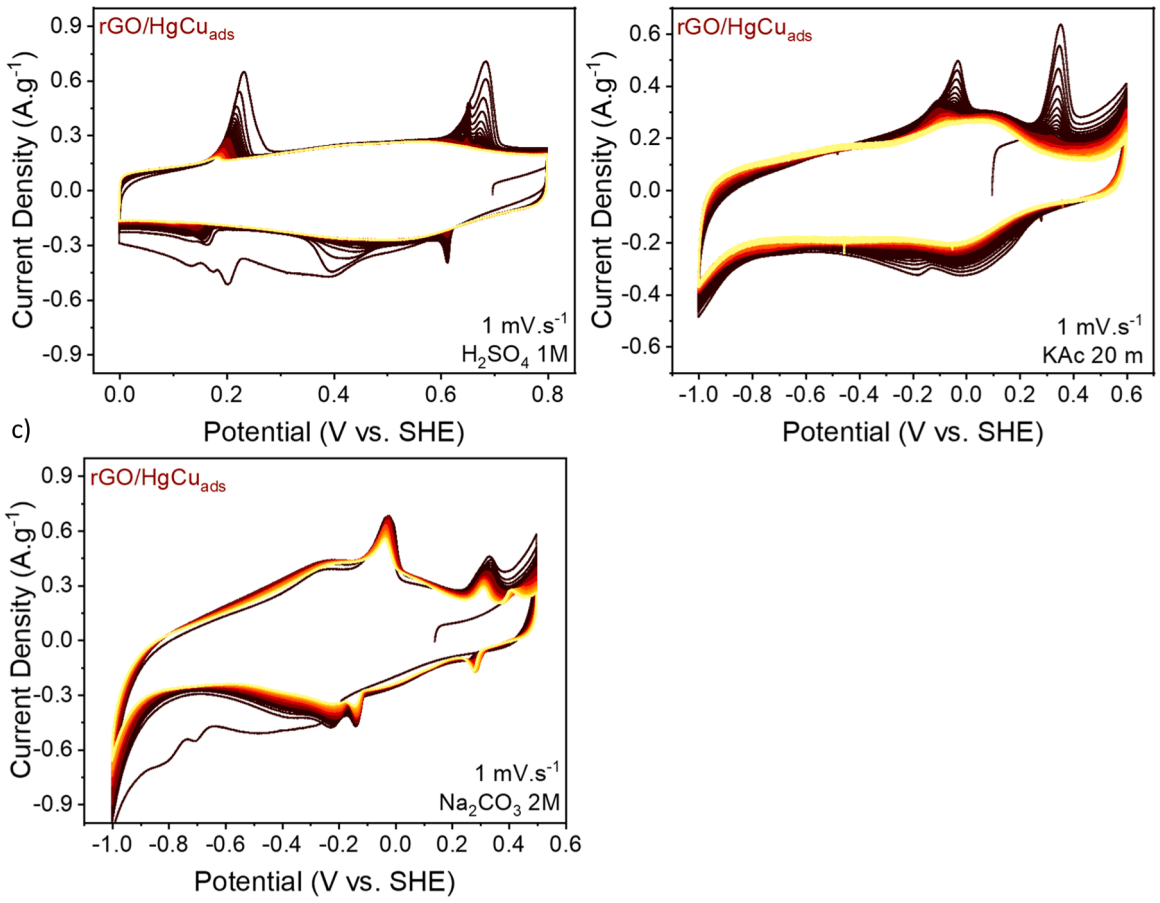

Fig. 6. Cyclic voltammetry at 1 mV·s^{-1} of rGO/HgCu$_{ads}$ in: a) 1 M H_2SO_4, b) 20 m Kac W, and c) 2 M Na_2CO_3.

Following acid treatment, the powder was rinsed with deionized (DI) water, approximately 250 mL per gram of MAX, until a neutral pH was achieved. The product was then filtered and dried at 60 °C. An etching solution was prepared by dissolving 4.8 g of lithium fluoride (LiF, >99 %, Honeywell Fluka) in 60 mL of 9 M HCl under continuous stirring for 5 min. 3 g of the pre-washed MAX powder was slowly introduced to the etchant. This mixture was stirred continuously at room temperature for 24 h. The acidic mixture was then subjected to three washing cycles using deionized water and centrifugation at 5000 rpm for 5 min per cycle. After each cycle, the supernatant was discarded and replaced with fresh DI water. The washing process was continued until the suspension reached a pH of approximately 5. The upper black $Ti_3C_2T_x$ slurry was collected using a spatula, resuspended in DI water, and centrifuged again at 2500 rpm for 5 min. The collected supernatant was then vacuum filtered and vacuum-dried at 80 °C for 24 h to obtain $Ti_3C_2T_x$ powder.

Materials characterization

Scanning Electron Microscopy & Energy Dispersive X-ray Spectroscopy. SEM images were obtained with a Zeiss Merlin instrument at 20 kV, and EDX analysis was conducted with an OXFORD Instruments device, 50 mm^2 X-Max detector at an 8 mm working distance.

Electrochemistry

Electrode Preparation. Recycled adsorbent electrodes were fabricated using either pristine adsorbent materials (rGO or $Ti_3C_2T_x$) or adsorbents loaded with heavy metals (such as rGO/Hg$_{ads}$, $Ti_3C_2T_x$/Cu$_{ads}$, rGO/Cu$_{ads}$, rGO/Pb$_{ads}$, or rGO/HgCu$_{ads}$) as the active components. The active materials were rinsed with deionized water and freeze-dried overnight. For electrode preparation, the active material was mixed with carbon black (PUREBLACK 205–110 Carbon, Superior Graphite Co.) and PTFE binder (60 % w/w aqueous solution, Sigma Aldrich) in a weight ratio of 70:20:10. The mixture was then dispersed in ethanol and homogenized using a SpeedMixer (FlackTek™ 515–200 PRO) at 2500 rpm for 3 min. The resulting paste was cold-rolled into freestanding films approximately 100 μm thick using a glass rod. Circular electrodes of 8 mm in diameter were then punched from these films.

For the thick activated carbon (AC) counter electrodes, a mixture was prepared using AC YP50, 10 % carbon black (PUREBLACK 205–110 Carbon, Superior Graphite Co., Chicago, IL, USA), and 5 % PTFE binder (60 % w/w aqueous solution, Sigma Aldrich), all dispersed in ethanol, mixed at 2500 rpm and dried. A film of around 1 mm in thickness was opened with a glass rod, and self-supporting AC electrodes with a 12 mm diameter were cut from the dried material.

Cell Assembly. Swagelok-type cells were used for all electrochemical characterizations. For cyclic voltammetry studies, the 3-electrode setup included a self-standing working electrode, two glass microfiber separators (GF-D 1172–4113, Fisherbrand), and an AC counter electrode, with excess electrolyte, with a reference electrode (Hg/Hg_2SO_4 in sat. K_2SO_4) placed in the third aperture. For GCPL, the counter thick AC electrode was replaced with a self-standing adsorbent-derived electrode of interest. All values reported in V *vs.* SHE were calculated using the actual reference electrode potential of + 0.635 V *vs.* SHE.

Measurements. Cyclic voltammetry and galvanostatic charge/discharge were performed using a VMP3 potentiostat (Biologic, operated under ECLab software version V11.50) in an air-conditioned room (22 °C).

Conclusions

This study expands the concept of directly repurposing spent wastewater adsorbents into functional energy storage devices through the electrochemical behavior of various heavy metal cations in various electrolytes. Our findings demonstrate that the adsorption of redox-active heavy metals brings tunable faradaic contributions that synergistically merge with the pristine capacitance, improving the total capacities.

Beyond the initial proof-of-concept, we demonstrate how newly explored adsorbents and adsorbates, including Pb^{2+}, Cu^{2+}, and multi-cation combinations, such as Hg^{2+} and Cu^{2+}, significantly expand the tunability of redox activity of recycled rGO and MXene-based electrodes, with the former being superior for both adsorption of Cu^{2+}cations and as electrodes. Furthermore, the coupling of different adsorbed cations enables the tuning of the voltage plateau, and we also present the assembly and evaluation of full cells using recycled metal-loaded adsorbents as both positive and negative electrode materials.

The unique electrochemistry of each cation is also determined by the choice of electrolyte, influencing how effectively the redox activity can be used. Furthermore, the capacity fading, caused by cation dissolution, is also electrolyte-dependent and improved upon by multiple and quite different types of aqueous electrolytes, although not yet completely mitigated.

Overall, this study paves the way for a new class of multifunctional materials derived from environmental waste streams, offering both ecological remediation and alternative energy solutions.

CRediT authorship contribution statement

Marcelo A. Andrade: Writing – original draft, Visualization, Methodology, Investigation, Formal analysis. **Olivier Crosnier:** Writing – review & editing, Supervision, Conceptualization. **Patrik Johansson:** Writing – review & editing, Validation. **Thierry Brousse:** Writing – review & editing, Supervision, Project administration, Conceptualization.

Declaration of competing interest

The authors declare the following financial interests/personal relationships which may be considered as potential competing interests:

Marcelo Amaro de Andrade reports financial support was provided by European Commission Marie Sklodowska-Curie Actions. Marcelo Amaro de Andrade reports financial support was provided by Conseil Régional des Pays de la Loire and Labex STORE-EX (ANR-10-LABX-76–01). Patrik Johansson reports financial support was provided by Swedish Research Council. If there are other authors, they declare that they have no known competing financial interests or personal relationships that could have appeared to influence the work reported in this paper.

Acknowledgements

As a part of the DESTINY Ph.D. program, this publication is acknowledged by funding from the European Union's Horizon2020 research and innovation program under the Marie Skłodowska-Curie Actions COFUND (Grant Agreement #945357). Conseil Régional des Pays de la Loire is also acknowledged for supporting this Ph.D. project, as well as Labex STORE-EX (ANR-10-LABX-76–01). The authors are also grateful for the financial support from the Swedish Research Council (VR) Distinguished Professor grant 'Next Generation Batteries' (#2021-00613). The authors would like to acknowledge the support of their colleague Camille Douard for all the cooperative work done.

Supplementary materials

Supplementary material associated with this article can be found, in the online version, at doi:10.1016/j.electacta.2025.147176.

Data availability

Data will be made available on request.

References

[1] V. Singh, et al., Toxic heavy metal ions contamination in water and their sustainable reduction by eco-friendly methods: isotherms, thermodynamics and kinetics study, Sci. Rep. 14 (2024) 1–13.
[2] T. Velempini, M.E.H. Ahamed, K. Pillay, Heavy-metal spent adsorbents reuse in catalytic, energy and forensic applications- a new approach in reducing secondary pollution associated with adsorption, Result. Chem. 5 (2023) 100901.
[3] F.S. Awad, K.M. Abouzeid, W.M.A. El-Maaty, A.M. El-Wakil, M.S. El-Shall, Efficient removal of heavy metals from polluted water with high selectivity for mercury(II) by 2-imino-4-thiobiuret-partially reduced graphene oxide (IT-PRGO), ACS Appl. Mater. Interface. 9 (2017) 34230–34242.
[4] Q. Li, et al., MXenes-based adsorbents for environmental remediation, Sep. Purif. Technol. 342 (2024) 126982.
[5] Z. Othman, H.R. Mackey, K.A. Mahmoud, A critical overview of MXenes adsorption behavior toward heavy metals, Chemosphere 295 (2022) 133849.
[6] Z. Tan, et al., Cu-doped porous carbon derived from heavy metal-contaminated sewage sludge for high-performance supercapacitor electrode materials, Nanomaterials 9 (2019) 1–14.
[7] Z. Chen, et al., Recycling spent water treatment adsorbents for efficient electrocatalytic water oxidation reaction, Resour. Conserv. Recycl. 178 (2022) 106037.
[8] D.A. Gkika, A.C. Mitropoulos, G.Z. Kyzas, Why reuse spent adsorbents? The latest challenges and limitations, Sci. Total Environ. 822 (2022) 153612.
[9] J. Ma, C. Liu, Turning waste into treasure: reuse of contaminant-laden adsorbents (Cr(VI)-Fe3O4/C) as anodes with high potassium-storage capacity, J. Colloid Interface Sci. 582 (2021) 1107–1115.
[10] M.A. Andrade, O. Crosnier, P. Johansson, T. Brousse, Energy from garbage: recycling heavy metal-containing wastewater adsorbents for Energy storage, Adv. Energy Sustain. Res. 2400195 (2024).
[11] Y. Zhang, L. Wang, N. Zhang, Z. Zhou, Adsorptive environmental applications of MXene nanomaterials: a review, RSC Adv. 8 (2018) 19895–19905.
[12] M. Ghidiu, M.R. Lukatskaya, M.-Q. Zhao, Y. Gogotsi, M.W. Barsoum, Conductive two-dimensional titanium carbide 'clay' with high volumetric capacitance, Nature 516 (2014) 78–81.
[13] M. Hu, et al., Intensifying electrochemical activity of Ti3C2Tx MXene via customized interlayer structure and surface chemistry, Molecules 28 (2023).
[14] S. Wee, et al., Tuning MXene properties through Cu intercalation: coupled guest/host redox and pseudocapacitance, ACS Nano 18 (2024) 10124–10132.
[15] M.-H. Kim, K.-B. Kim, S.-M. Park, K.C. Roh, Hierarchically structured activated carbon for ultracapacitors, Sci. Rep. 6 (2016) 21182.
[16] R.A. Lenin, et al., Ecofriendly fabrication and theoretical insights of ascorbic acid assisted rGO electrodes for high performance solid state supercapacitors, Sci. Rep. 15 (2025) 26318.
[17] Y. Zhang, et al., N/O co-enriched graphene hydrogels as high-performance electrodes for aqueous symmetric supercapacitors, RSC Adv. 11 (2021) 19737–19746.
[18] V.L. Martins, R.M. Torresi, Water-in-salt electrolytes for high voltage aqueous electrochemical energy storage devices, Sci. Rep. 5 (2020) 100901.
[19] A. Shahzad, et al., Two-dimensional Ti3C2Tx MXene nanosheets for efficient copper removal from water, ACS Sustain. Chem. Eng. 5 (2017) 11481–11488.
[20] X. Sang, et al., Atomic defects in monolayer titanium carbide (Ti3C2Tx) MXene, ACS Nano 10 (2016) 9193–9200.
[21] P. Liu, C.J. Ptacek, D.W. Blowes, R.C. Landis, Mechanisms of mercury removal by biochars produced from different feedstocks determined using X-ray absorption spectroscopy, J. Hazard. Mater. 308 (2016) 233–242.
[22] L. Largitte, R. Pasquier, A review of the kinetics adsorption models and their application to the adsorption of lead by an activated carbon, Chem. Eng. Res. Des. 109 (2016) 495–504.
[23] M.A. Andrade, et al., Tracking Hg2+ adsorption by reduced graphene oxide in continuous flow by *in situ* techniques, J. Environ. Chem. Eng. (2025), https://doi.org/10.1016/j.jece.2025.118680.
[24] C. Zhan, et al., Understanding the MXene pseudocapacitance, J. Phys. Chem. Lett. 9 (2018) 1223–1228.
[25] N. Takeno, Atlas of eh-pH diagrams. National Institute of Advanced Industrial Science and Technology, Geological Survey of Japan, 2005.
[26] R.K. Jena, H.T. Das, B.N. Patra, N. Das, MXene-based nanomaterials as adsorbents for wastewater treatment: a review on recent trends, Front. Mater. Sci. 16 (2022) 1–16.
[27] Q. Peng, et al., Unique lead adsorption behavior of activated hydroxyl group in two-dimensional titanium carbide, J. Am. Chem. Soc. 136 (2014) 4113–4116.
[28] X. Xie, et al., Microstructure and surface control of MXene films for water purification, Nat. Sustain. 2 (2019) 856–862.
[29] M.A. Andrade, et al., Synthesis of 2D solid-solution (NbyV2-y)CTx MXenes and their transformation into oxides for energy storage, ACS Appl. Nano Mater. 6 (2023) 16168–16178.
[30] M. Downes, C.E. Shuck, B. McBride, J. Busa, Y. Gogotsi, Comprehensive synthesis of Ti3C2Tx from MAX phase to MXene, Nat. Protoc. 19 (2024) 1807–1834.